Photoemission and optical studies of $ZrSe_3$, $HfSe_3$, and ZrS_3

D. Pacilé,[1,2] M. Papagno,[1,2] M. Lavagnini,[3] H. Berger,[4] L. Degiorgi,[3] and M. Grioni[1]
[1]*Ecole Polytechnique Fédéderale de Lausanne, Institut de Physique des Nanostructures, CH-1015 Lausanne, Switzerland*
[2]*Istituto Nazionale di Fisica Nucleare (INFN), Dipartimento di Fisica, Università della Calabria, 87036 Rende, Cosenza, Italy*
[3]*Laboratorium für Festkörperphysik, ETH Zürich, CH-8093 Zürich, Switzerland*
[4]*Ecole Polytechnique Fédéderale de Lausanne, Institut de Physique de la Matière Complexe, CH-1015 Lausanne, Switzerland*
(Received 12 February 2007; revised manuscript received 16 May 2007; published 4 October 2007)

Angle-resolved photoemission spectroscopy (ARPES) and optical measurements were performed on single crystal samples of $ZrSe_3$, $HfSe_3$, and ZrS_3, which belong to the class of low-dimensional band insulators. By ARPES, we traced the dispersion of the (S $3p$, Se $4p$) p-derived valence states. In all cases, the topmost band exhibits energy splitting increasing from S to Se, which we attribute to the spin-orbit interaction, similar to recent observations in the related layered dichalcogenides. The combination of optical and photoemission results allows us to address the issue of the gap feature in the absorption spectra and to characterize the electronic and vibrational properties of $ZrSe_3$, $HfSe_3$, and ZrS_3.

DOI: 10.1103/PhysRevB.76.155406 PACS number(s): 71.45.Lr, 78.20.−e, 79.60.−i

I. INTRODUCTION

Low-dimensional correlated systems have become, over the past two decades, primary centers of interest in condensed matter research. Among them, quasi-one-dimensional materials have been under intense scrutiny because of their spin- and charge-density-wave instabilities.[1,2] Furthermore, characteristic deviations from Fermi liquid behavior are expected in one-dimensional (1D) systems, as well as unusual phenomena associated with the formation of the broken-symmetry ground states. The trichalcogenides MX_3, where M is a group IVB or VB transition metal, and X is S, Se, or Te, are typical examples of this class of materials.[3,4] Metallic $ZrTe_3$ and $NbSe_3$, for example, exhibit charge-density-wave transitions, leading to distinctive changes of the Fermi surface and of the spectral response, which have been thoroughly investigated in recent angle-resolved photoelectron spectroscopy (ARPES) and optical experiments.[5–8] In the present paper, by contrast, we address the electronic structure of $ZrSe_3$, $HfSe_3$, and ZrS_3, three diamagnetic semiconducting members of the same family which do not exhibit lattice distortions. These compounds provide us with an opportunity to investigate possible effects of low dimensionality in a band insulator, i.e., a system that is insulating at all temperatures on the basis of crystal periodicity and electron counting.

The MX_3 chalcogenides crystallize in several related, usually monoclinic, structures. All of them contain infinite parallel chains of trigonal prismatic MX_6 units that are at the origin of their strongly anisotropic physical properties. The group IV compounds considered here belong to the $ZrSe_3$ structural type (Fig. 1, top), with two identical chains per unit cell, running along the crystallographic b axis and offset by $b/2$.[9] The S and Se atoms in the triangular bases of the prisms are not equivalent. One side of the triangle is much shorter than the other two (2.35 Å vs 3.75 Å and 3.79 Å in $ZrSe_3$), implying the formation of a Se-Se or S-S bond. This is confirmed by x-ray photoemission spectra which show a splitting of the chalcogen core levels, indicative of chemically inequivalent sites.[10] The presence of bonded chalcogen pairs differentiates the chemical bonding in the trichalcogenides from that of the related and much studied dichalcogenides.[11] The valence state of these compounds can therefore be described as $M^{4+}(X_2^{2-})X^{2-}$, even if this ionic description is only approximate, and covalency is certainly non-negligible. The overlap of the Zr (Hf) $4d_{z^2}$ ($5d_{z^2}$) orbitals along the b axis leads to the formation of a band with marked 1D character, which lies above the Fermi level E_F. The character of the S (Se) valence bands is more isotropic due to the short distance (3.06 Å in $ZrSe_3$) between neighboring chains along the a axis. This distance is intermediate between the short and long sides in the base of the prisms. The chains are arranged in double layers parallel to the a-b plane, which are weakly coupled by van der Waals bonds. The crystals can be cleaved easily at the van der Waals gap to expose atomically flat (001) surfaces.

The available information on the electronic structure of these semiconducting compounds is rather limited in comparison with the metallic sister compounds. On the theory side, the band structure of $ZrSe_3$ has been calculated using a nonempirical atomic orbital method[12] or the Korringa-Kohn-Rostoker method.[13] Further useful indications can be deduced from more recent first-principles self-consistent calculations for the isostructural and isoelectronic $ZrTe_3$.[14,15] Spectroscopic data are also scarce. Valence band density of states has been measured in momentum-integrated photoemission experiments with limited energy resolution.[10,16] ARPES experiments have not yet been performed to determine the band dispersion. Similarly, only a few results are available on the optical properties, yet on limited spectral ranges.[17–26]

The goal of the present work is to present ARPES and optical results with improved resolution and over a very broad energy range, which will considerably extend our knowledge on the electronic structure of these materials. The combination of the two complementary data sets is important to obtain a complete picture of the dynamical properties. Optical spectroscopy is a bulk probe of the total charge density, while ARPES directly probes the dispersion of the occupied chalcogen (S, Se) p-derived valence band. We find

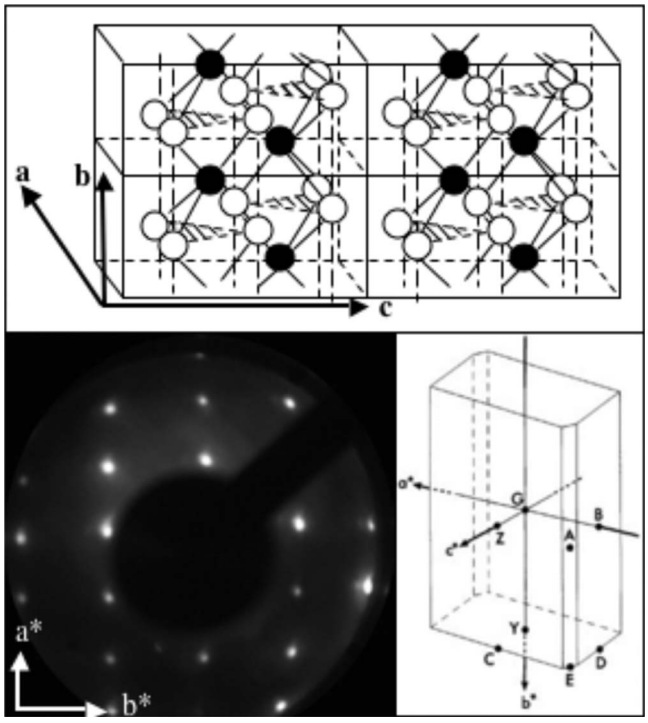

FIG. 1. (Top) The three-dimensional $ZrSe_3$ crystal structure, where infinite parallel chains of MX_6 prisms run along the b direction. The filled circles indicate the M cations. (Bottom, left) LEED image of the (001) cleavage plane. The arrows indicate the surface reciprocal lattice vectors. (Bottom, right) The three-dimensional Brillouin zone.

that, for all three materials, this band is similarly split into two nearly parallel subbands. Their energy separation increases from ZrS_3 to the Se compounds, pointing to the spin-orbit interaction as the likely origin of this splitting. Our optical findings allow us to address the phonon spectrum as well as the excitations due to the electronic interband transitions. A comparison between the ARPES results and the absorption spectrum raises the issue of the energy gap excitation in $ZrSe_3$, $HfSe_3$, and ZrS_3.

II. EXPERIMENT

Single crystals of $ZrSe_3$, $HfSe_3$, and ZrS_3 were grown by vapor-phase transport in the shape of large shiny platelets. Photoemission data were collected on samples freshly cleaved *in situ* at room temperature by a Scienta ESCA-300 spectrometer equipped with a high-brilliance monochromatized He lamp. The Fermi energy location and the total energy resolution ($\Delta E = 10$ meV) were separately determined from the metallic edge of a polycrystalline Ag film. The angular resolution was better than 1°. We utilized low-energy electron diffraction (LEED) to verify the sample orientation and surface quality. The LEED pattern of Fig. 1 is typical of a cleaved surface, showing the rectangular surface reciprocal lattice.

The optical reflectivity $[R(\omega)]$ was obtained from the far infrared (FIR) up to the ultraviolet (UV) with our variety of

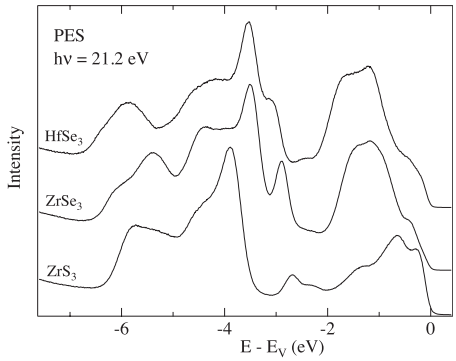

FIG. 2. Angle-integrated photoemission spectra of the valence bands of $ZrSe_3$, $HfSe_3$, and ZrS_3 ($h\nu = 21.2$ eV). The energy zero for each compound coincides with the estimated valence band maximum E_V.

spectrometers.[27] Light was polarized either parallel or perpendicular to the chain axis. The spectra for $ZrSe_3$ and ZrS_3 were collected in the whole available spectral range (i.e., FIR-UV, $30-5\times10^4$ cm^{-1}), those for $HfSe_3$ were collected only from the infrared up to the UV range (i.e., from 600 up to 5×10^4 cm^{-1}). We did not observe any temperature dependence of the optical response. The optical conductivity was calculated by the Kramers-Kronig (KK) transformation of the reflectivity spectra. To this end and because of the insulating behavior of $ZrSe_3$, $HfSe_3$, and ZrS_3, $R(\omega)$ was extrapolated to a constant value for $\omega \to 0$. For $HfSe_3$, we have neglected the IR active phonon modes and extrapolated its reflectivity to a constant value already below 600 cm^{-1}. This crude extrapolation has, however, no influences in the spectral range pertinent to the discussion of the gap excitation. At higher frequencies, on the other hand, the standard extrapolations $R(\omega) \sim \omega^{-s}$ $(2 \leqslant s \leqslant 4)$ were applied for all compounds. Details pertaining to the experiment and data analysis can be found in Refs. 28 and 29.

III. ANGLE-RESOLVED PHOTOEMISSION SPECTROSCOPY MEASUREMENTS

Figure 2 summarizes our angle-integrated photoemission results for the three materials, measured with He I excitation ($h\nu = 21.2$ eV). In order to facilitate a comparison of corresponding density of states (DOS) features in the three compounds, all spectra in this figure were aligned at the respective valence band maximum E_V. E_V was determined as usual by a linear extrapolation to the base line of the leading edge of each spectrum. The spectra are in general agreement with the calculated density of states[12,13] and with published angle-integrated data measured at the same photon energy,[16] but reveal finer details thanks to the better experimental resolution. They reflect valence states of S (Se) $3p$ ($4p$) character, with only limited Zr (Hf) $4d$ ($5d$) admixture, which explains the overall similarities and the one-to-one correspondence of all spectral features in the two Se compounds. According to the paired-anion ligands picture $M^{4+}(X_2^{2-})X^{2-}$, and with two formula units per unit cell, there are 32 S (Se) electrons to be placed in 16 of the 18 available $3p$ ($4p$) bands. The assign-

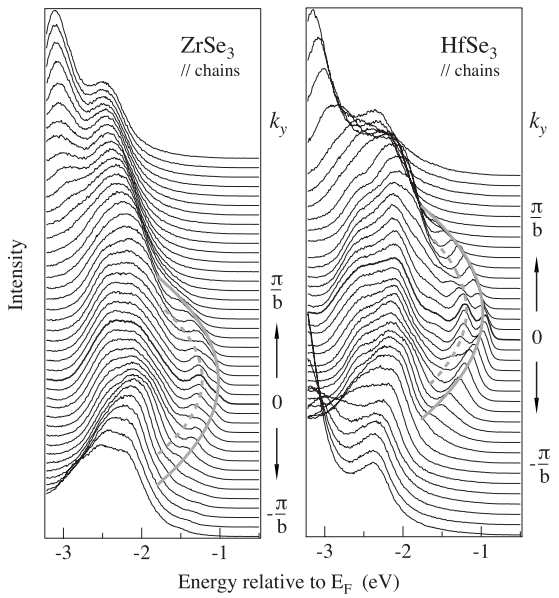

FIG. 3. ARPES spectra ($h\nu$=21.2 eV) of $ZrSe_3$ (left) and $HfSe_3$ (right) measured along the chain direction. The energy zero coincides with the Fermi level. Each curve refers to a different polar emission angle, and the angular step is 1°. Values of the wave vector k_y along the chains, evaluated at $E=E_F$, are indicated, with "0" corresponding to normal emission. Thick solid and dashed gray lines highlight the dispersion of two closely spaced subbands.

ment of the various DOS features has been discussed before,[10,12,16] but it is not totally unambiguous. The highest occupied states are derived from antibonding hybrid states of the X_2 group, of π_g^* symmetry, with cation p and d states, while the antibonding σ_u^* orbitals are empty.[10] Hybrid states between the X_2 and the cation s, p, and d orbitals, of σ_g and π_u characters, have been assigned to the more strongly bound peak at ~−6 eV and to one of the intermediate features at ~−3 eV. The remaining spectral components, e.g., the −0.8 eV peak in $ZrSe_3$, are attributed to states derived from unpaired anions. In the crystal, the actual situation is more subtle, and the interchain interaction along the a axis must be explicitly considered, as discussed in Ref. 14. For an ideal structure with a constant separation between the chains, the highest occupied and lowest unoccupied p bands would be degenerate at the zone boundary, and the material would be a semimetal. The semiconducting character is due to the alternation of short (d_1) and long (d_2) interchain distances, which leads to an energy gap between a $pp\sigma$ and a $pp\sigma^*$ band. Interestingly, when the d_2/d_1 ratio is close to 1, as in $ZrTe_3$ (1.11 vs 1.45 in ZrS_3), the gap is small. One of the Te 5p bands is then destabilized and raised above the bottom of the antibonding $pp\sigma^*$ band, thus yielding a metal.[14]

Figure 3 presents ARPES spectra of $ZrSe_3$ and $HfSe_3$, measured along the chains, i.e., along the ΓY direction in reciprocal space (Fig. 1, bottom) or, equivalently, along $\bar{\Gamma}\bar{Y}$ in the surface Brillouin zone (SBZ). The angular step was 1°. Both sets of data show weakly dispersing structures between −2 and −3 eV, and two closely spaced spectral features which rapidly disperse downwards in energy from their maxima (at ~−1 and −1.2 eV) at $\bar{\Gamma}$, the center of the SBZ.

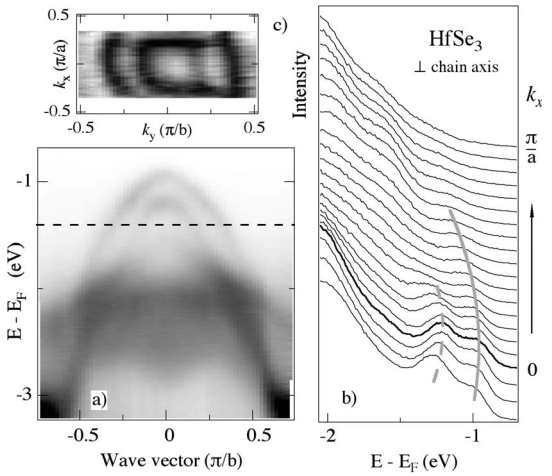

FIG. 4. (a) ARPES intensity map of $HfSe_3$, corresponding to the data in Fig. 3(b). (b) ARPES spectra ($h\nu$=21.2 eV) of $HfSe_3$ measured along the a axis, perpendicular to the chain direction. (c) A two-dimensional constant energy slice near the center of the Brillouin zone at E=−1.4 eV [dashed line in (a)].

Figure 4(a) gives an alternative representation of the $HfSe_3$ data as an ARPES intensity map. The measured ARPES intensity is displayed on a gray scale (largest intensity is black) as a function of wave vector and binding energy. Here, the parallel dispersion of the two subbands can be clearly appreciated. The rapidly dispersing ARPES features, which flatten out toward the zone boundary, clearly correspond to the broad chalcogen p_y band predicted by band structure calculations.[14,15] This band has a smaller but non-negligible dispersion along the perpendicular a axis. This is illustrated by the set of spectra in Fig. 4(b) and confirmed by the ARPES constant energy cut (at E=−1.4 eV) in Fig. 4(c). Even within the limited momentum window of the data, the rounded shape of the contour clearly indicates that this band has not a 1D character. The weakly dispersing bands can be attributed to a dense p manifold with some admixture of metal d states.[14,15]

For ZrS_3, the overall band structure is also similar, as shown in the ARPES intensity map in Fig. 5. The main difference is a smaller (~70 meV) energy separation between the two subbands at the $\bar{\Gamma}$ point. The ARPES results for the topmost valence band of the three compounds are summarized in the right panel of Fig. 5. The lines are cosine functions interpolating the experimental (E,k) data points, which were extracted from the individual ARPES spectra by a Gaussian line shape analysis of the dispersing spectral features. The figure shows that the band dispersion, including the energy separation between the two subbands, is essentially determined by the chalcogen. From the dispersions, we have estimated for each compound the effective masses m^* of the pair of subbands at the Γ point. The resulting values are $(0.7m_0;0.4m_0)$ for $ZrSe_3$; $(0.8m_0;0.4m_0)$ for $HfSe_3$; and $(1.0m_0;0.4m_0)$ for ZrS_3. The first value in the parentheses refers to the shallower subband and the second one to the deeper subband; m_0 is the free electron mass.

As to the origin of the splitting of the topmost valence band, we notice that this characteristic feature of the band

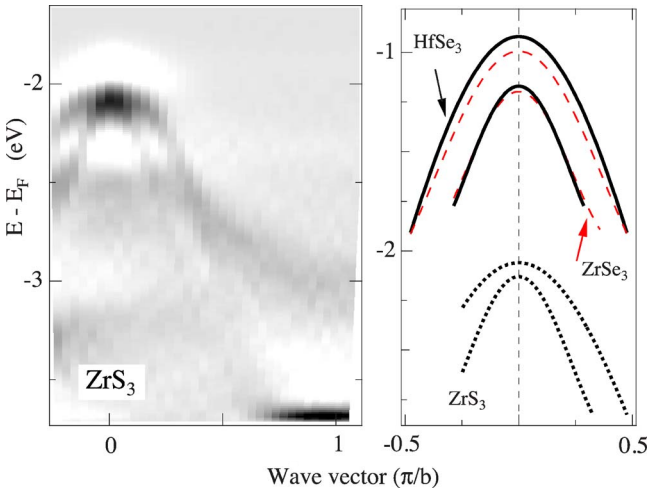

FIG. 5. (Color online) (Left) ARPES intensity map of ZrS_3 along the $\overline{\Gamma Y}$ chain direction ($h\nu$=21.2 eV). (Right) The dispersion of the top valence subbands in the chain direction, as determined from the ARPES data: $HfSe_3$ (solid lines), $ZrSe_3$ (red dashed lines), and ZrS_3 (dotted line).

structure is not present in the available calculations.[13–15] A crucial hint is provided by recent ARPES measurements of the dichalcogenides $1T-TaS_2$ and $1T-TaSe_2$, where similarly split bands were observed.[30] The splitting was absent in the nonrelativistic band structures, but could be reproduced by scalar-relativistic calculations, pointing to the spin-orbit (SO) interaction as the likely origin of the effect. The experimental energy separation at the band maximum was found to be close to the atomic S $3p$ value [95 meV (Ref. 31)] for $1T-TaS_2$ and to half of the atomic Se $4p$ splitting [418 meV (Ref. 31)] for $1T-TaSe_2$, and the latter reduced value was assigned to hybridization in the solid state. We propose here an analogous interpretation, which is indeed strengthened by the similarity of the results in structurally different materials. We also observe a similar reduction of the SO splitting with respect to the atomic value, which is marginal for ZrS_3 and substantial in the Se compounds. This again is indicative of a larger metal-anion hybridization in the latter, consistent with the more delocalized nature of the Se $4p$ orbitals.

IV. OPTICAL MEASUREMENTS

Figures 6(a) and 7(a) present the measured $R(\omega)$ of ZrS_3 and $ZrSe_3$ for both polarizations. Figures 6(b) and 7(b) and Figs. 6(c) and 7(c) display the real part $\sigma_1(\omega)$ of the complex optical conductivity for light polarized parallel and perpendicular to the chains, respectively. At high frequencies ($\omega > 3000\ cm^{-1}$), we recognize the onset of rather strong absorption features, which will be later ascribed to electronic interband transitions, particularly in terms of the fundamental energy gap excitation. The FIR spectral range is characterized by sharp absorptions [see also insets of Figs. 6(a) and 7(a)], typical for phonon mode excitations. Our data agree fairly well with previous optical findings.[17–26] However, our optical spectra are collected on a much broader and extended

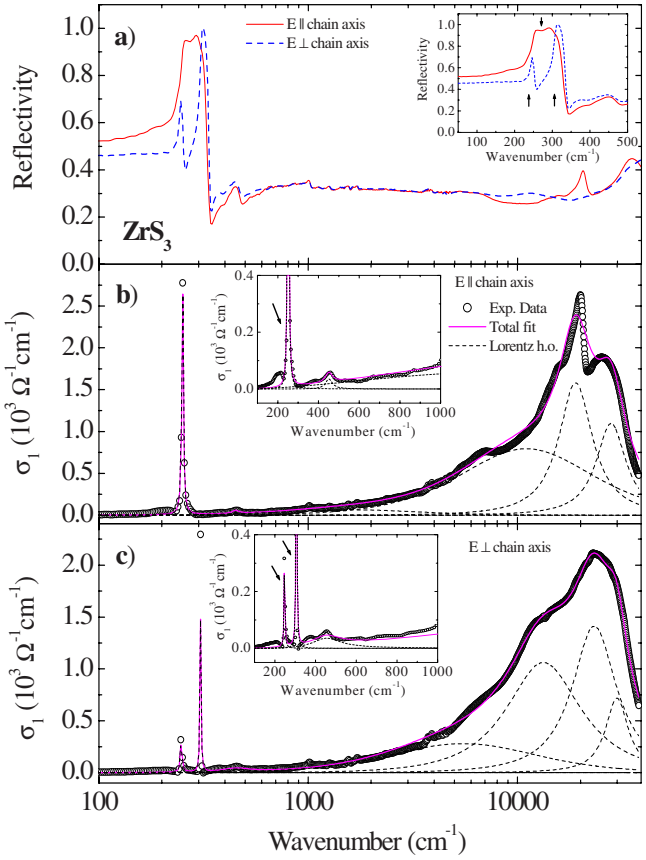

FIG. 6. (Color online) (a) Optical reflectivity $R(\omega)$ at 300 K along both polarization directions for ZrS_3. The inset shows the FIR spectral range with the IR active phonon modes. [(b) and (c)] $\sigma_1(\omega)$ of ZrS_3 for light polarized parallel and perpendicular to the chains, respectively, with the total Lorentz fit and the corresponding components (see text). The insets in (b) and (c) are a blowup of the FIR spectral range.

spectral range than in the past, significantly improving the data reliability and quality.

There is an obvious anisotropy in the optical spectra, along and perpendicular to the chains with respect to both phonon excitations and electronic transitions. This is very much indicative of the low dimensionality of the systems. In order to facilitate and to better support the discussion below, we describe the experimental findings within the Lorentz phenomenological approach.[28,29] It consists of an adequate number of Lorentz harmonic oscillators (h.o.'s), describing the various absorptions in the spectra. The total fit and the corresponding components are highlighted in Figs. 6(b) and 7(b) and Figs. 6(c) and 7(c) for ZrS_3 and $ZrSe_3$, respectively.

A. Phonon analysis

The phenomenological fit of $R(\omega)$ and $\sigma_1(\omega)$ in terms of Lorentz h.o.'s allows us to precisely determine the resonance frequencies ω_{0i} for the IR active phonon modes (arrows in the insets of Figs. 6 and 7). Those frequencies compare well with the position of the peak maximum in the imaginary part ϵ_2 of the complex dielectric function.[28,29] The ω_{0i} frequen-

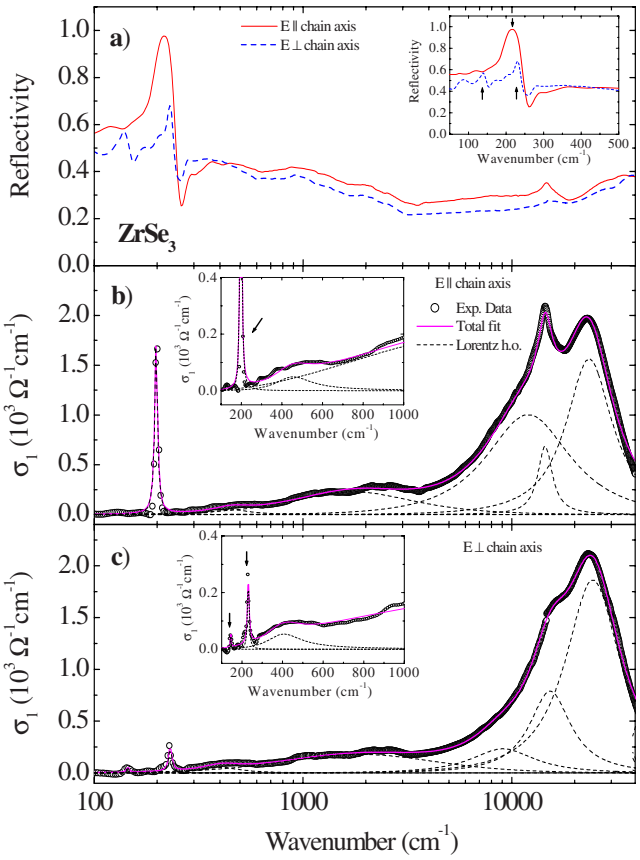

FIG. 7. (Color online) (a) Optical reflectivity $R(\omega)$ at 300 K along both polarization directions for $ZrSe_3$. The inset shows the FIR spectral range with the IR active phonon modes. [(b) and (c)] $\sigma_1(\omega)$ of $ZrSe_3$ for light polarized parallel and perpendicular to the chains, respectively, with the total Lorentz fit and the corresponding components (see text). The insets in (b) and (c) are a blowup of the FIR spectral range.

cies are summarized in Table I and physically correspond to the transverse optical phonon frequencies ω_{TO}. The Lyddane-Sachs-Teller relation $\epsilon_\infty = \epsilon_0(\omega_{TO}^2/\omega_{LO}^2)$ provides a simple way to estimate the related longitudinal optical phonon mode frequencies ω_{LO}. To this end, the static (ϵ_0) and optical (ϵ_∞) dielectric constants were estimated from the real part ϵ_1 of the dielectric function. This is done in two ways: (i) directly from the experimental ϵ_1, obtained from the KK transformation of $R(\omega)$, by looking at the values of ϵ_1 on the high and low frequency tails of the phonon resonance at ω_{0i}, and (ii) by calculating ϵ_0 and ϵ_∞ within the Lorentz fit close to the phonon absorption. ϵ_0 turns out to be the static limit $\epsilon_1(\omega \to 0)$ of the phonon resonance, while ϵ_∞ is actually the static limit, provided by all resonances placed at frequencies above the excitation at any given ω_{TO}. While both ways give equivalent results, we apply here the second one which guarantees a more precise estimation of ω_{LO}. The resulting ω_{LO} are summarized in Table I with the related values of ϵ_0 and ϵ_∞.

Our findings agree very well with the results and the analysis of a previous investigation.[21,23,24] On the one hand, the C_{2h} (monoclinic) symmetry of $ZrSe_3$, $HfSe_3$, and ZrS_3 allows the $3A_1$ modes of the chains to appear in the perpendicular direction, although the A_1 resonances are expected to be weak. On the other hand, the measured spectra perpendicular to the chains [Figs. 6(a) and 7(a)] do exhibit two narrow bands of B_u symmetry, which we attribute to the principal B_2 internal modes of the chain. The weak feature between 400 and 500 cm^{-1} could correspond to the $B_u(A_1)$ diatomic mode.[21] For the direction parallel to the chains, the measured spectra clearly display one single broad Reststrahlen-like feature, which can be associated with the strong $A_u(B_1)$ rigid-sublattice mode, polarized along the chain axis.[21]

B. Electronic interband transitions

The strong absorption features in $\sigma_1(\omega)$ for all compounds, whose broad onset occurs above about 3000 cm^{-1}, are emphasized in Fig. 8 using a linear energy scale. Along the chains, we find a well pronounced peak located at ω_{max}, which seems to be a characteristic feature of each compound [see arrows in Fig. 8(a)]. Indeed, there is an indication of a dependence of ω_{max} on both the transition metal M and the chalcogens X, the latter being stronger. This latter peak is accompanied by a broader feature at about 2.5×10^4 cm^{-1} for all compounds. For light polarized perpendicular to the chains [Fig. 8(b)], on the other hand, there is a broad absorption, whose maximum depends almost exclusively on the transition element. At least for the Zr compounds, we additionally identify a kink on the low frequency side of ω_{max} (i.e., at approximately 1×10^4 and 1.5×10^4 cm^{-1} for the S and Se compounds, respectively). Below 3000 cm^{-1}, there is a rather broad low frequency tail, extending from about 600 up to 5000 cm^{-1} for both polarizations [Figs. 6(b), 6(c), 7(b), 7(c), and 8]. Such a broad midinfrared part could represent the excitations due to so-called midgap states, possibly asso-

TABLE I. Resonance frequencies ω_{0i} of the IR active transverse phonon modes for both polarizations, obtained from the Lorentz fit of $ZrSe_3$ and ZrS_3. The longitudinal phonon mode frequencies ω_{0i}^{LO} are calculated by the Lyddane-Sachs-Teller relation (see text), making use of the corresponding ϵ_0 and ϵ_∞ values. All frequencies are given in cm^{-1}. The reader should note that along the chain, there is no second mode.

Samples	ω_{01}	$\omega_{01}^{(LO)}$	$\epsilon_0^{(1)}$	$\epsilon_\infty^{(1)}$	ω_{02}	$\omega_{02}^{(LO)}$	$\epsilon_0^{(2)}$	$\epsilon_\infty^{(2)}$
$ZrSe_3$ (∥)	198	264	46.9	26.4				
$ZrSe_3$ (⊥)	145	147	28.3	27.6	231	239	27.6	25.9
ZrS_3 (∥)	251	334	31.8	18.0				
ZrS_3 (⊥)	248	257	22.3	20.7	306	339	20.7	16.9

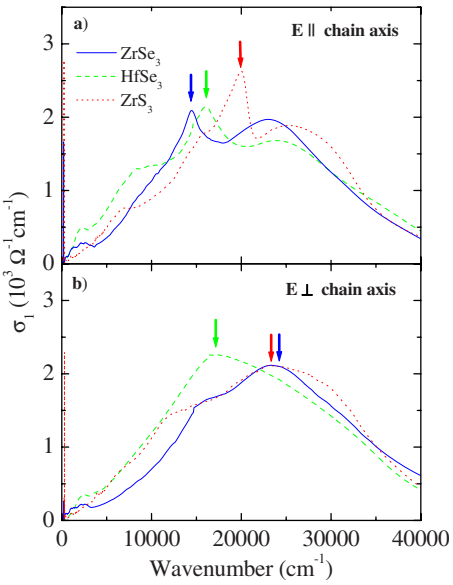

FIG. 8. (Color online) $\sigma_1(\omega)$ at 300 K for $ZrSe_3$, $HfSe_3$, and ZrS_3 for light polarized (a) along and (b) perpendicular to the chains, respectively. The arrows indicate ω_{max} (see text and Table II).

ciated with defects or vacancies.[32] Previous scanning tunneling microscopy work reported charge instability between various selenium and/or tellurium chains forming at the surface and possibly related to excess chalcogenide concentration.[33]

The Lorentz model is a rather common tool for getting further insight on the spectra and particularly for extracting the characteristic absorption energy scales. For all compounds, we account for the spectral range above 600 cm^{-1} with a broad Lorentz h.o., describing the midinfrared tail of the interband transitions, and three h.o.'s for the strong absorption features above 3000 cm^{-1} (Figs. 6 and 7). These latter h.o.'s have a merely phenomenological meaning and allow recovering the broad absorption, peaked at ω_{max}. The corresponding resonance frequencies of the Lorentz h.o.'s are summarized in Table II. Missing the support of a detailed band structure calculation, it would be too speculative and beyond the scope of the Lorentz fit to assign each single h.o. to a distinct electronic transition. In contrast to our previous work on $NbSe_3$,[7] where an assignment of each h.o. was somehow more feasible and reliable, it is here more appropriate to introduce a weighted energy scale $\tilde{\omega}=\frac{\sum_{j=1}^{3}\omega_j S_j^2}{\sum_{j=1}^{3}S_j^2}$; the sum is over the three high frequency h.o.'s at resonance energies ω_j, S_j being their respective mode strengths.[34] $\tilde{\omega}$ phenomenologically identifies the relevant energy scale associated with the optical excitation peaked at ω_{max}. Interestingly enough, $\tilde{\omega}$ of all compounds coincides fairly well with the experimentally determined peak energy ω_{max} (Table II) and such a satisfactory comparison gives us confidence in our phenomenological approach based on the Lorentz model.

Previous optical investigations have already addressed the estimation of the (fundamental) energy gap, yet leading to a large interval of values.[17–20,22,25,26] Particularly, as far as the early reports are concerned, this unsatisfactory situation originates from the limited covered spectral range. In the very first optical absorption work, Grimmeiss *et al.* extracted the direct energy gap values of 2.2 and 1.2 eV for ZrS_3 and $ZrSe_3$, respectively.[17] Using an extrapolation method from diffuse reflectance spectra, Brattas and Kjekshus obtained the values for the band gaps of 1.95 eV for ZrS_3 and of 1.91 eV for $ZrSe_3$.[18] The most reliable of the early optical work is that by Schairer and Shafer, who performed optical absorption measurements on single crystals and reported a fundamental optical gap value of 2.8 eV for ZrS_3, corresponding to an allowed direct transition.[19] In the early 1980s, Bayliss and Liang performed reflectivity measurements, extracting a direct gap of about 1.9 eV in $ZrSe_3$,[22] while Perluzzo *et al.* found a direct gap exciton of ~2.5 eV in ZrS_3.[20] The more recent optical investigation by Kurita *et al.* reports an exciton direct allowed transition at 2.6 and 1.82 eV for ZrS_3 and $ZrSe_3$, respectively.[25] Therefore, the latest optical data seem to converge toward values for the energy gap of about 2.6 eV for ZrS_3 and 1.9 eV for $ZrSe_3$. This is in very good agreement and matches quite well with the energy scales ω_{max} and $\tilde{\omega}$ along the chains extracted from our comprehensive optical results (Table II and Fig. 8).

It is worth mentioning that Khumalo and Hughes proposed from high energy reflection spectroscopy and based on simple physical and chemical arguments as well as molecular orbital ideas that the optical excitation across the energy gap occurs between the occupied p states and the d-state conduction band.[26] They proposed that the lowest unoccupied state has d_{z^2} character, i.e., polarized along the chain. In fact, ω_{max}

TABLE II. Resonance frequencies ω_i and corresponding mode strength S_i for the Lorentz harmonic oscillators, describing the absorptions in $\sigma_1(\omega)$ above 5000 cm^{-1} for $ZrSe_3$, $HfSe_3$, and ZrS_3, and both polarizations. ω_{max} are the frequencies locating the peak position in $\sigma_1(\omega)$ (arrows in Fig. 8). The weighted energy $\tilde{\omega}$ scales (see text) are reported, as well. All entries are in units of 10^4 cm^{-1}.

Samples	ω_1	S_1	ω_2	S_2	ω_3	S_3	$\tilde{\omega}$	ω_{max}
$ZrSe_3$ (∥)	1.20	2.87	1.50	1.07	2.35	3.70	1.90	1.45
ZrS_3 (∥)	1.10	3.20	1.90	2.84	2.80	2.70	1.84	2.00
$HfSe_3$ (∥)	0.90	2.77	1.60	2.00	2.56	3.41	1.85	1.61
$ZrSe_3$ (⊥)	0.91	1.04	1.53	2.01	2.45	4.47	2.24	2.33
ZrS_3 (⊥)	1.33	2.91	2.33	3.41	2.99	1.97	2.08	2.30
$HfSe_3$ (⊥)	0.98	2.07	1.76	4.03	2.73	2.26	1.82	1.71

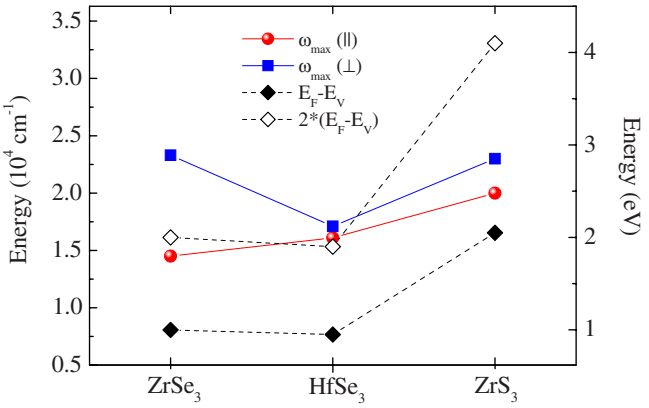

FIG. 9. (Color online) Comparison of the optical energy scale ω_{max} for both polarizations and the quantities (E_F-E_V) and $2(E_F-E_V)$ from ARPES (see text). The lines are guides for the eyes.

along the perpendicular direction are at higher values than along the chain. Displaying different energy gaps along orthogonal polarization directions is, by the way, a common feature of anisotropic materials.[1,7] Furthermore, the ARPES data [e.g., Figs. 3 and 4(b)] clearly show that the occupied p states in the valence bands are isotropic, therefore implying that the systems are truly two dimensional. Consequently, the important anisotropy in the optical response between the two polarization directions (Fig. 8) must originate from the highly orientation dependent unoccupied d states. Finally, Khumalo and Hughes pointed out that the band structures of the Zr compounds are very closely similar except that the $ZrSe_3$ conduction bands are 0.6 eV lower with respect to the main ZrS_3 valence band.[26] This is in good agreement with the difference between our optical energy gap values along the chain for both compounds (Table II).

The measured ARPES dispersion (Figs. 4 and 5) yields, for all three materials, the energy position of the valence band maximum E_V with respect to the Fermi level E_F. The E_V values thus determined coincide with those extracted from a linear extrapolation of the leading edge of the momentum-integrated spectra of Fig. 2. Figure 9 summarizes the values of the quantity (E_F-E_V) from ARPES, along with the optical energy gap ω_{max} for both polarization directions. Assuming that the Fermi level E_F is located in the middle of the p-d gap, as for an intrinsic semiconductor, the gap size should be approximately equal to twice the ARPES gap (E_F-E_V). On the other hand, minute concentrations of defects or impurities, well below the ARPES sensitivity level, can cause the chemical potential to swing across the gap.[35] Therefore, the possibility that E_F is pinned near the conduction band minimum E_C by donor levels cannot be *a priori* excluded [pinning by acceptor levels is ruled out by the large (E_F-E_V) values]. Donor levels have actually been reported, e.g., in $ZrSe_3$ at $\sim$0.25 eV below E_C.[32] In this case, the ARPES (E_F-E_V) would be close to the entire gap. The lower limit (E_F-E_V) and the upper limit $2(E_F-E_V)$ of the estimated gap from the ARPES data are indicated by the dashed lines in Fig. 9. For $ZrSe_3$ and $HfSe_3$, we find that the optical energy gap essentially coincides with $2(E_F-E_V)$. For ZrS_3, on the other hand, the optical gap is close to the ARPES lower limit. This suggests that in this particular case, the Fermi level was indeed pinned near E_C by donors. We emphasize, however, that a definitive test of this hypothesis would require an independent probe of the unoccupied states, like inverse photoemission spectroscopy (IPES). Indeed, only an analysis of the optical spectrum in light of both the occupied (ARPES) and unoccupied (IPES) band structures would remove the uncertainties on the origin of the individual optical transitions, which were treated here phenomenologically.

V. CONCLUSIONS

We performed angle-resolved photoemission and optical measurements on single crystal samples of three low-dimensional band insulators: $ZrSe_3$, $HfSe_3$, and ZrS_3. The ARPES results illustrate the dispersion of the chalcogen-derived $3p$ $(4p)$ valence bands, and are consistent with band structure calculations which assign a rather two-dimensional character to these bands. We find, however, that the highest occupied band of all compounds is split into two almost parallel subbands, whose energy separation increases from S to Se. We assign this splitting to the result of the spin-orbit interaction.

Unlike photoemission, the optical measurements probe transitions into unoccupied bands, derived from both metal and chalcogen states, for which theory predicts a marked 1D character. Indeed, the absorption spectrum is highly anisotropic, as far as both phonon modes and electronic transitions are concerned. This justifies a low-dimensional (quasi-1D) scenario for the lattice, and even more for the electronic properties of these materials. While the comparison between optics and ARPES sheds some light on the relevant energy scales, the determination of the fundamental energy gap is yet not conclusive. A separate knowledge on the unoccupied states would be necessary in order to fully and unambiguously reconcile the findings from both spectroscopies. This is actually an outstanding issue of more general interest. As a future perspective, it would therefore be quite interesting to complement the present data with angle-resolved inverse photoemission measurements, which can directly and selectively probe the quasi-1D unoccupied cation bands.

ACKNOWLEDGMENTS

The authors wish to thank J. Müller for technical help and A. Sacchetti for fruitful discussions. This work has been supported by the Swiss National Foundation for Scientific Research and by the NCCR MaNEP.

[1] G. Grüner, *Density Waves in Solids* (Addison-Wesley, Reading, MA, 1994).
[2] *Strong Interactions in Low Dimensions*, edited by D. Baeriswyl and L. Degiorgi (Kluwer Academic, Dordrecht, 2004).
[3] A. Meerschaut and J. Rouxel, in *Crystal Chemistry and Properties of Materials with Quasi-one-dimensional Structures*, edited by J. Rouxel (Reidel, Dordrecht, 1986), p. 205.
[4] W. Kroenert and K. Plieth, Z. Anorg. Allg. Chem. **336**, 207 (1965).
[5] J. Schäfer, M. Sing, R. Claessen, E. Rotenberg, X. J. Zhou, R. E. Thorne, and S. D. Kevan, Phys. Rev. Lett. **91**, 066401 (2003).
[6] T. Yokoya, T. Kiss, A. Chainani, S. Shin, and K. Yamaya, Phys. Rev. B **71**, 140504(R) (2005).
[7] A. Perucchi, L. Degiorgi, and R. E. Thorne, Phys. Rev. B **69**, 195114 (2004).
[8] A. Perucchi, L. Degiorgi, and H. Berger, Eur. Phys. J. B **48**, 489 (2004).
[9] S. Furuseth, L. Brattas, and A. Kjekshus, Acta Chem. Scand., Ser. A **29**, 623 (1975).
[10] F. Jellinek, R. A. Pollak, and M. W. Shafer, Mater. Res. Bull. **9**, 845 (1974).
[11] J. A. Wilson, F. J. Di Salvo, and J. Mahajan, Adv. Phys. **24**, 117 (1975).
[12] D. W. Bullet, J. Phys. C **12**, 277 (1979).
[13] H. W. Myron, B. N. Harmon, and F. S. Khumalo, J. Phys. Chem. Solids **42**, 263 (1981).
[14] K. Stöwe and F. R. Wagner, J. Solid State Chem. **138**, 160 (1998).
[15] C. Felser, E. W. Finckh, H. Kleinke, F. Rocker, and W. Tremel, J. Mater. Chem. **8**, 1787 (1998).
[16] G. Margaritondo, A. D. Katnani, N. G. Stoffel, and F. Levy, J. Electron Spectrosc. Relat. Phenom. **20**, 69 (1980).
[17] H. G. Grimmeiss, A. Rabenau, H. Hahn, and P. Ness, Z. Elektrochem. **65**, 776 (1961).
[18] L. Brattas and A. Kjekshus, Acta Chem. Scand. (1947-1973) **25**, 2783 (1973).
[19] W. Schairer and M. W. Shafer, Phys. Status Solidi A **17**, 181 (1973).
[20] G. Perluzzo, S. Jandl, and P. E. Girard, Can. J. Phys. **58**, 143 (1980).
[21] A. Grisel, F. Lévy, and T. J. Wieting, Physica B & C **99B**, 365 (1980).
[22] S. C. Bayliss and W. Y. Liang, J. Phys. C **14**, L803 (1981).
[23] J. Deslandes and S. Jandl, Phys. Rev. B **29**, 2088 (1984).
[24] S. Jandl, M. Banville, and J.-Y. Harbec, Phys. Rev. B **22**, 5697 (1980).
[25] S. Kurita, M. Tanaka, and F. Lévy, Phys. Rev. B **48**, 1356 (1993).
[26] F. S. Khumalo and H. P. Hughes, Phys. Rev. B **22**, 2078 (1980).
[27] A. Schwartz, M. Dressel, G. Grüner, V. Vescoli, L. Degiorgi, and T. Giamarchi, Phys. Rev. B **58**, 1261 (1998).
[28] M. Dressel and G. Grüner, *Electrodynamics of Solids* (Cambridge University Press, Cambridge, England, 2002).
[29] F. Wooten, *Optical Properties of Solids* (Academic, New York, 1972).
[30] F. Clerc, M. Bovet, H. Berger, L. Despont, C. Koitzsch, O. Gallus, L. Patthey, M. Shi, J. Krempasky, M. G. Garnier, and P. Aebi, J. Phys.: Condens. Matter **16**, 3271 (2004).
[31] F. Herman and S. Skillman, *Atomic Structure Calculations* (Prentice-Hall, Englewood Cliffs, NJ, 1963).
[32] T. Ikari, R. Provencher, S. Jandl, and M. Aubin, Solid State Commun. **45**, 113 (1983).
[33] A. Prodan, V. Marinkovic, N. Jug, H. J. P. van Midden, H. Böhm, F. W. Boswell, and J. C. Bennett, Surf. Sci. **482-485**, 1368 (2001).
[34] A. Sacchetti, L. Degiorgi, T. Giamarchi, N. Ru, and I. R. Fisher, Phys. Rev. B **74**, 125115 (2006).
[35] See, e.g., L. J. Brillson, Surf. Sci. Rep. **2**, 123 (1982).